

Single-crystal *in situ* high-temperature structural investigation of the $\bar{I}1$ – $I2/c$ phase transition in $\text{Ca}_{0.2}\text{Sr}_{0.8}\text{Al}_2\text{Si}_2\text{O}_8$ feldspar

PIERA BENNA* AND EMILIANO BRUNO

Dipartimento di Scienze Mineralogiche e Petrologiche, Via Valperga Caluso 35, I-10125 Torino, and Istituto di Geoscienze e Georisorse, CNR, Sezione di Torino, Italy

ABSTRACT

Structural modifications induced by the $\bar{I}1$ – $I2/c$ displacive transition in $\text{Ca}_{0.2}\text{Sr}_{0.8}\text{Al}_2\text{Si}_2\text{O}_8$ feldspar ($\text{An}_{20}\text{SrF}_{80}$) have been investigated *in situ* by single-crystal X-ray diffraction at 20, 200, 400, 500, and 620 °C. Crystals were synthesized from the melt, cooled slowly to 1300 °C, and then quenched in air. At room temperature ($a = 8.361$, $b = 12.973$, $c = 14.259$ Å, $\alpha = 90.79$, $\beta = 115.55$, $\gamma = 90.62^\circ$, $V = 1394.9$ Å³; space group: $\bar{I}1$; $Q_{\text{od}} = 0.88$), the polyhedra of the non-tetrahedral cation have different configurations at the Ca/Sr(0) and Ca/Sr(z) sites. In monoclinic Sr feldspar, the Sr-O_B and Sr-O_D distances are regular, but in triclinic $\text{An}_{20}\text{SrF}_{80}$ feldspar the O_B(m0) atom in the Ca/Sr(0)-polyhedron and the O_D(mz) atom in the Ca/Sr(z)-polyhedron are displaced. The topochemical symmetry of the framework is essentially monoclinic and the average dimensions of the pseudo-symmetrical tetrahedra do not change within the error limits. With increasing temperature, the distances between the Ca/Sr cations and the pseudo-related O atom pairs converge on the values adopted at the $\bar{I}1$ – $I2/c$ transition. At the transition point, the M-polyhedron assumes a regular coordination, similar to that observed in monoclinic Sr feldspar at room temperature. The results obtained indicate $T_{\text{tr}} = 520 \pm 10$ °C, in agreement with the transition temperature obtained from the changes of cell dimensions. The variation of $\cos^2\alpha^*$ with temperature is consistent with the solution to Landau 2-4-6 potential with $T_c = 506 \pm 7$ °C.

INTRODUCTION

It is known that complete solid solution occurs between $P\bar{I}$ anorthite (An) and $I2/c$ strontium feldspar (SrF) along the $\text{CaAl}_2\text{Si}_2\text{O}_8$ – $\text{SrAl}_2\text{Si}_2\text{O}_8$ join. At room temperature, the $P\bar{I}$ – $\bar{I}1$ phase transition occurs near $\text{An}_{50}\text{SrF}_{50}$ (Phillips et al. 1997; Tribaudino et al. 2000). The triclinic-monoclinic, $\bar{I}1$ – $I2/c$, phase transition occurs at $\sim\text{An}_{10}\text{SrF}_{90}$ in samples with high degrees of Al/Si order (Bruno and Gazzoni 1968; Nager 1969; Nager et al. 1969; Tribaudino et al. 1993; McGuinn and Redfern 1994; Dove and Redfern 1997). In the Sr-rich region of the join, feldspars with compositions between $\text{An}_{40}\text{SrF}_{60}$ and $\text{An}_{10}\text{SrF}_{90}$ are triclinic at room temperature, but undergo the analogous $\bar{I}1$ – $I2/c$ transition on heating. The $\bar{I}1$ – $I2/c$ transition is a zone-center, displacive ferroelastic transition. Whereas single-crystal structural refinements at room and high-temperature are available for the Ca and Sr end-members (Megaw et al. 1962; Czank 1973; Foit and Peacor 1973; Chiari et al. 1975; Benna and Bruno 2001), only unit-cell parameters, obtained by powder X-ray diffraction (XRD) at room and high-temperature, are available for feldspars of intermediate compositions along the An-SrF join (Bruno and Gazzoni 1968; Nager et al. 1970; Bambauer and Nager 1981; Tribaudino et al. 1993; McGuinn and Redfern 1997). Following the recent synthesis from melt of crystals of composition $\text{An}_{20}\text{SrF}_{80}$, large enough for single-crystal XRD, we report the results obtained by intensity collection from room

temperature to $T = 620$ °C. The objective of this study was to define the structural modifications that take place with increasing temperature and, in particular, to examine the modifications occurring when monoclinic symmetry is achieved.

EXPERIMENTAL METHODS

The starting material was a gel of stoichiometric $\text{Ca}_{0.20}\text{Sr}_{0.80}\text{Al}_2\text{Si}_2\text{O}_8$ composition, prepared according to the method of Biggar and O'Hara (1969). The gel was treated in a molybdenum disilicide (MoSi₂) furnace, equipped with high-stability digital temperature controllers, programmed cooling and heating cycles, using unsealed tubes of platinum (Pt-Pt Rh 30% thermocouple). The sample was melted and annealed at $T = 1680$ °C for 1 h and then cooled at a constant rate (60 °C/h) to 1300 °C, with subsequent quenching in air. Crystals larger than 100 µm were obtained.

Powder XRD (Imaging Plate Guinier Camera, Huber 670, $\lambda = 1.5406$ Å, quartz as internal standard), revealed that $\text{An}_{20}\text{SrF}_{80}$ feldspar was the only crystallizing phase. Unit-cell parameters obtained by powder XRD are shown in Table 1. For comparison, the values obtained by Nager et al. (1969) and McGuinn and Redfern (1997) are also reported. Minor differences can be ascribed to small compositional variations caused by the different methods of preparation of starting materials or to the different synthesis conditions (temperatures and times of treatment), which could have caused different degrees of Al/Si order in the samples (Tribaudino et al. 1993).

Transmission electron microscopy (TEM) was performed using a Philips CM-12 electron microscope operating at 120 kV and equipped with double-tilt goniometer stage. The sample was crushed in an agate mortar and then deposited on a holey carbon film. Selected-area electron diffraction (SAED) patterns showed both *a*-type ($h + k = 2n$, $l = 2n$) and sharp *b*-type superstructure reflections ($h + k = 2n + 1$, $l = 2n + 1$). No *c*-type ($h + k = 2n$, $l = 2n + 1$) and *d*-type ($h + k = 2n + 1$, $l = 2n$) reflections were observed. The $\text{An}_{20}\text{SrF}_{80}$ feldspar therefore has an *I* lattice, and space group $\bar{I}1$ was assumed, according to Phillips et al. (1997) and Tribaudino et al. (2000). Dark-field images display polysynthetic twinning that can be interpreted according to the albite law (Fig. 1). In SAED

* E-mail: piera.benna@unito.it

TABLE 1. Unit-cell parameters of $\text{An}_{20}\text{SrF}_{80}$ feldspar (e.s.d. in brackets)

a (Å)	b (Å)	c (Å)	α (°)	β (°)	γ (°)	V (Å ³)
(1) 8.356(2)	12.963(2)	14.249(3)	90.86(1)	115.51(1)	90.65(1)	1392.5
(2) 8.351(1)	12.965(1)	14.242(3)	91.00(1)	115.48(2)	90.75(1)	1391.5
(3) 8.359(1)	12.967(1)	14.248(1)	90.74(1)	115.49(1)	90.56(1)	1393.6

Notes: (1) Nager et al. (1969); (2) McGuinn and Redfern (1997); (3) this work (Guinier Camera).

patterns, albite twins are easily detected by the splitting of reflections parallel to b^* . Albite twins develop during cooling as a consequence of the loss of the mirror plane caused by the $I2/c$ - $I1$ transition. The average diameter of type b antiphase domains is 400 Å, extending up to ~1000 Å in some cases. The heterogeneity of b domain sizes probably can be connected to crystallization from the melt and to the relatively short time of cooling. Such heterogeneity is not observed in samples isothermally treated at high-temperature for sufficiently long times (Benna et al. 1995).

A twin-free crystal chosen for data collection ($0.10 \times 0.06 \times 0.05$ mm) was fixed to a quartz glass fiber by GA-100 HT cement. Single-crystal XRD was performed in situ at $T = 20, 200, 400, 500$, and 620 °C. Intensities were collected with a Siemens P4 four-circle diffractometer, using graphite-monochromatized $\text{MoK}\alpha$ radiation ($\lambda = 0.7107$ Å) in the θ - 2θ scan mode. A U-shaped heating furnace was employed for high- T single-crystal diffraction, with K-type thermocouple and a Series 988 Watlow Temperature Controller. The position of the crystal was 4 mm from the tip of the thermocouple. The set temperatures show a discrepancy with respect the actual sample temperatures, which are always higher. A correction to the set temperature was performed according to Mott, Klitrø, and He (Bruker Internal Report). The temperature error of the furnace was estimated to be ± 10 °C at 500 °C. Diffractometer angles for the same set of 40 reflections were collected for unit-cell parameter refinements at intervals of about 100 °C. Reflections ($-h, \pm k, \pm l$) up to $2\theta = 70^\circ$ were measured with a variable scanning speed (2.4–30 °/min). An empirical absorption correction, based on the ψ -scan method (North et al. 1968) at room temperature, was used for all data sets because, at higher temperatures, the heating attachment prevented measurement of the required ψ -scans. Data were corrected for background and Lorentz-polarization effects using the SHELXTL-Plus 1990 system (Sheldrick 1997). A weighting scheme was used for the data only at the end of refinement cycles. In all data sets, a and b reflections were collected. For the temperature range 20–500 °C, space group $I1$ was assumed, and at $T = 620$ °C, space group $I2/c$ was assumed. Reflections with $F_o \geq 2\sigma(F_o)$ were regarded as observed and used in the refinements.

Table 2 contains the observed and calculated structure factors¹. Unit-cell parameters, refinement data, atomic fractional coordinates, and displacement parameters are given in Tables 3, 4, and 5, respectively. Relevant interatomic distances are listed in Tables 6 and 7.

RESULTS AND DISCUSSION

The structure of $\text{An}_{20}\text{SrF}_{80}$ at room temperature

Substitution of Ca for Sr induces triclinic symmetry in $\text{An}_{20}\text{SrF}_{80}$ feldspar, characterized by a significant distortion of the Ca/Sr-polyhedron. In detail, the polyhedron of the non-tetrahedral cation assumes different configurations at the Ca/Sr(0) and Ca/Sr(z) sites, as it is evident from the M-O bond lengths in Table 6. Although the M-O_A(1) and M-O_A(2) distances show small changes in comparison with the values observed in monoclinic Sr feldspar, significant modifications occur in the M-O_B, M-O_D, and M-O_C distances. Modifications to the M-O_B and M-O_D distances are well represented in Figure 2, which shows

partial projections of the feldspar structure on the (100) plane. Whereas in monoclinic Sr feldspar the Sr-O_B and Sr-O_D distances are regular, in triclinic $\text{An}_{20}\text{SrF}_{80}$ feldspar marked displacements of the O_B(m0) atom in the Ca/Sr(0)-polyhedron and

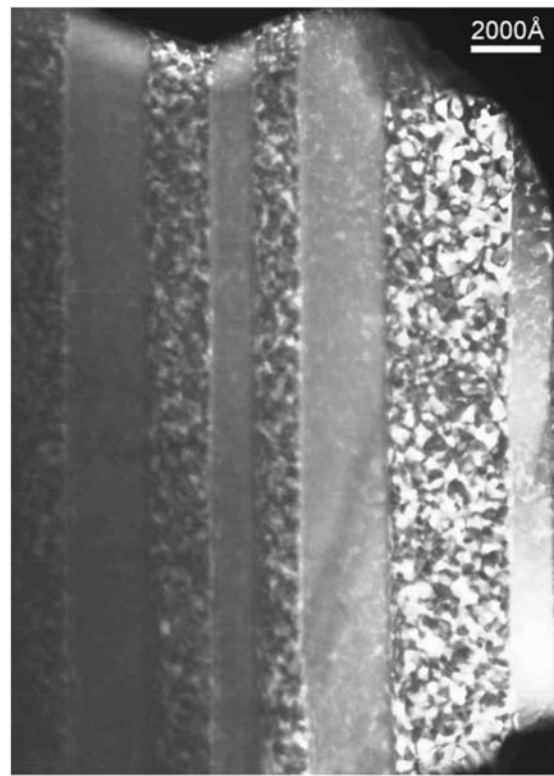


FIGURE 1. $\text{An}_{20}\text{SrF}_{80}$ feldspar. Dark-field image of albite twin. Type b antiphase domains are imaged in only one set of lamellae; $\mathbf{g} = \bar{5}25$.

TABLE 3. Unit-cell parameters at different temperatures (single-crystal)

T (°C)	a (Å)	b (Å)	c (Å)	α (°)	β (°)	γ (°)	V (Å ³)
20	8.361(1)	12.973(2)	14.259(2)	90.79(1)	115.55(1)	90.62(1)	1394.9
200	8.367(1)	12.968(2)	14.266(2)	90.68(1)	115.51(1)	90.54(1)	1396.8
300	8.372(1)	12.970(2)	14.274(2)	90.64(1)	115.49(1)	90.35(1)	1398.8
400	8.377(1)	12.971(2)	14.275(2)	90.46(1)	115.49(1)	90.30(1)	1399.9
500	8.379(2)	12.971(3)	14.278(2)	90.11(1)	115.48(2)	90.06(2)	1400.8
550	8.383(1)	12.972(2)	14.283(2)	90.	115.50(1)	90.	1402.0
600	8.386(1)	12.973(2)	14.284(1)	90.	115.46(1)	90.	1403.0
620	8.386(1)	12.970(2)	14.283(1)	90.	115.46(1)	90.	1402.8

TABLE 4. Single-crystal data at different temperatures

	20	200	400	500	620
Space group	$\bar{I}\bar{I}$	$\bar{I}\bar{I}$	$\bar{I}\bar{I}$	$\bar{I}\bar{I}$	$\bar{I}\bar{I}/c$
μ (mm ⁻¹)	6.97	6.96	6.95	6.94	6.93
Refl. measured	7381	8605	7205	7721	6721
Unique refl.	6060	6083	6064	6072	3079
Refl. observed $F_o \geq 2\sigma(F_o)$	4823	4564	4147	4134	2215
Refl. b -type	1969	1812	1518	1508	834
No. refl. b / No. refl. a	0.688	0.656	0.576	0.574	0.604
$\sum F_{o(b)}^2 / \sum F_{o(a)}^2$	0.045	0.039	0.036	0.035	0.030
R	0.049	0.055	0.069	0.076	0.059
wR^2	0.099	0.109	0.138	0.171	0.124
Goodness of fit	1.05	1.02	1.03	1.00	1.01
R^*	0.36	0.30	0.19	0.08	0.06*

Notes: $w = 1 / [\sigma^2(F_o^2) + (0.1R)^2]$, where $R = (F_o^2 + F_c^2) / 3$. R^* (Winter et al. 1979) = $(\sum |F_h k l| - |\bar{F} h \bar{k} l|) / (\sum |F_h k l|)$.

* Triclinic model.

¹ For a copy of Table 2, Document AM-03-043, contact the Business Office of the Mineralogical Society of America (see inside front cover of recent issue) for price information. Deposit items may also be available on the American Mineralogist web site at <http://www.minsocam.org>.

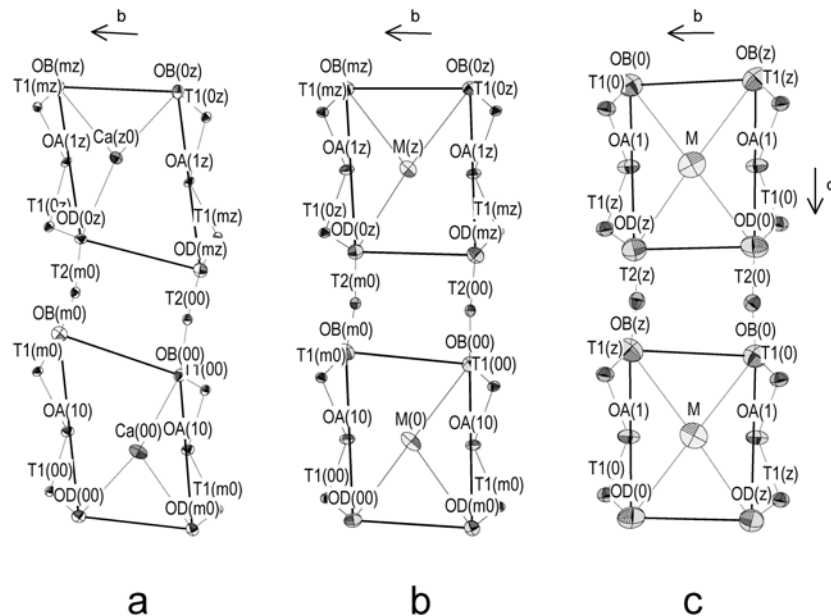


FIGURE 2. Partial coordination of the non-tetrahedral cation. Projection on the (100) plane: (a) anorthite, space group $P\bar{1}$, Kalus (1978); (b) $\text{An}_{20}\text{SrF}_{80}$ feldspar at $T = 20^\circ\text{C}$, space group $I\bar{1}$; (c) $\text{An}_{20}\text{SrF}_{80}$ feldspar at $T = 620^\circ\text{C}$, space group $I2/c$. Heavy solid line: $\text{O}_\text{B}-\text{O}_\text{D}$ quadrilaterals.

of the $\text{O}_\text{D}(\text{mz})$ atom in the $\text{Ca}/\text{Sr}(\text{z})$ -polyhedron are observed. With the release of one of the four O atoms at the vertex, the two $\text{O}_\text{B}(\text{m}0)-\text{O}_\text{B}(00)-\text{O}_\text{B}(\text{m}0)-\text{O}_\text{D}(00)$ and $\text{O}_\text{B}(\text{mz})-\text{O}_\text{B}(0z)-\text{O}_\text{D}(\text{mz})-\text{O}_\text{D}(0z)$ quadrilaterals (Fig. 2b), lying approximately on (100) (Bruno and Facchinelli 1974; Megaw 1974; Benza et al. 1996), deform significantly. This deformation of the $\text{O}_\text{B}-\text{O}_\text{D}$ quadrilaterals is related to the “collapse” induced by the decrease in the average dimension of the M cation and, therefore, to the $I2/c-I\bar{1}$ transition. In particular, the α angle (90.79°) is directly correlated with the deformation of the quadrilaterals in the (100) plane. The same “collapsed” configuration, with more developed deformation, is observed in anorthite for the $\text{Ca}(00)$ and $\text{Ca}(\text{z}0)$ polyhedra (Fig. 2a) and for the $\text{Ca}(\text{o}i)$ e $\text{Ca}(\text{z}i)$ polyhedra. Modifications in the $\text{M}-\text{O}_\text{C}$ distances are clearly shown in the partial projection of the structure of $\text{An}_{20}\text{SrF}_{80}$ feldspar on the (001) plane (Fig. 3). Significant lengthening of the $\text{M}-\text{O}_\text{C}(00)$ and $\text{M}-\text{O}_\text{C}(0z)$ distances and reduction of the $\text{M}-\text{O}_\text{C}(\text{m}0)$ and $\text{M}-\text{O}_\text{C}(\text{mz})$ distances are observed (Fig. 3a), in comparison to monoclinic Sr feldspar (Fig. 3b). Distortion of the Ca/Sr -polyhedron in the (001) plane is related to the variation of the γ angle (Bruno and Facchinelli 1974; Kroll and Müller 1980), which, in triclinic $\text{An}_{20}\text{SrF}_{80}$ feldspar, assumes the value of 90.62° . In anorthite, analogous modifications are observed, but they occur to a greater extent.

In addition to the changes in the Ca/Sr -polyhedron and in the $\text{Ca}/\text{Sr}-\text{O}$ distances, significant modifications to the $\text{T}-\text{O}-\text{T}$ angles occur. As observed by Chiari et al. (1978) in anorthite, there is a correlation between the $\text{M}-\text{O}$ distances and the $\text{T}-\text{O}_\text{B}-\text{T}$ and $\text{T}-\text{O}_\text{D}-\text{T}$ angles. With the increase of the $\text{M}-\text{O}_\text{B}(\text{m}0)$ and $\text{M}-\text{O}_\text{D}(\text{mz})$ distances, the $\text{T}-\text{O}_\text{B}(\text{m}0)-\text{T}$ and $\text{T}-\text{O}_\text{D}(\text{mz})-\text{T}$ angles also widen (Fig. 2b).

Regarding the framework of $\text{An}_{20}\text{SrF}_{80}$, collapse from the monoclinic structure to the triclinic structure, causes the change from the 4 independent T sites under monoclinic symmetry to 8 T sites under triclinic symmetry. The average dimensions of

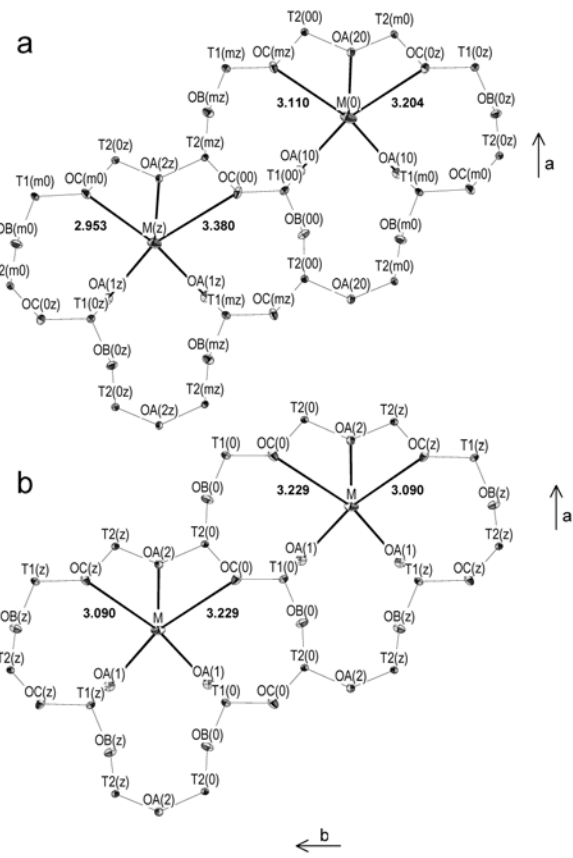


FIGURE 3. Partial coordination of the non-tetrahedral cation. Projection on the (001) plane: (a) $\text{An}_{20}\text{SrF}_{80}$ feldspar, space group $I\bar{1}$; (b) Sr-feldspar, space group $I2/c$, Benza and Bruno (2001). The $\text{M}-\text{O}_\text{C}$ distances (\AA) are indicated.

TABLE 5. Atomic fractional coordinates ($\times 10^4$), equivalent isotropic and anisotropic displacement coefficients ($\text{\AA}^2 \times 10^3$)

Site	x	y	z	U_{eq}	U_{11}	U_{22}	U_{33}	U_{12}	U_{13}	U_{23}
T = 20 °C										
Ca/Sr(0)	2694(1)	14(1)	669(1)	20(0)	8(0)	28(0)	22(0)	0(0)	3(0)	-11(0)
Ca/Sr(z)	2678(1)	72(1)	5629(1)	16(0)	8(0)	20(0)	17(0)	0(0)	4(0)	-3(0)
T ₁ (00)	70(1)	1698(1)	1072(1)	10(0)	9(0)	11(0)	9(0)	-3(0)	5(0)	0(0)
T ₁ (0z)	29(1)	1737(1)	6154(1)	9(0)	10(0)	10(0)	9(0)	-2(0)	5(0)	0(0)
T ₁ (m0)	22(1)	8194(1)	1176(1)	9(0)	10(0)	10(0)	9(0)	1(0)	5(0)	0(0)
T ₁ (mz)	68(1)	8222(1)	6095(1)	9(0)	9(0)	11(0)	8(0)	2(0)	4(0)	1(0)
T ₂ (00)	6919(1)	1185(1)	1669(1)	9(0)	8(0)	8(0)	10(0)	0(0)	3(0)	0(0)
T ₂ (0z)	6830(1)	1112(1)	6681(1)	9(0)	8(0)	8(0)	11(0)	-1(0)	4(0)	0(0)
T ₂ (m0)	6844(1)	8852(1)	1754(1)	9(0)	8(0)	8(0)	10(0)	0(0)	4(0)	0(0)
T ₂ (mz)	6927(1)	8781(1)	6724(1)	8(0)	8(0)	8(0)	10(0)	0(0)	4(0)	0(0)
O _A (10)	64(3)	1279(2)	9978(2)	14(0)	17(1)	17(1)	9(1)	-3(1)	7(1)	0(1)
O _A (1z)	9945(3)	1287(2)	4966(2)	13(0)	14(1)	16(1)	10(1)	2(1)	8(1)	2(1)
O _A (20)	5884(3)	9965(2)	1421(2)	13(0)	12(1)	8(1)	18(1)	0(1)	6(1)	2(1)
O _A (2z)	5874(3)	9967(2)	6422(2)	13(0)	10(1)	8(1)	19(1)	-1(1)	6(1)	2(1)
O _B (00)	8251(3)	1190(2)	1012(2)	16(0)	13(1)	17(1)	21(1)	-4(1)	11(1)	-1(1)
O _B (0z)	8061(3)	1194(2)	6067(2)	15(0)	15(1)	17(1)	18(1)	-3(1)	11(1)	0(1)
O _B (m0)	8100(4)	8675(2)	1174(2)	18(0)	15(1)	22(1)	24(1)	3(1)	13(1)	-3(1)
O _B (mz)	8275(3)	8679(2)	6087(2)	16(0)	14(1)	20(1)	18(1)	5(1)	11(1)	2(1)
O _C (00)	148(3)	2924(2)	1242(2)	16(0)	15(1)	13(1)	19(1)	-6(1)	7(1)	-4(1)
O _C (0z)	193(3)	3047(2)	6381(2)	16(0)	15(1)	12(1)	20(1)	-6(1)	7(1)	-3(1)
O _C (m0)	144(3)	6865(2)	1229(2)	15(0)	14(1)	11(1)	19(1)	3(1)	6(1)	1(1)
O _C (mz)	94(3)	6979(2)	6119(2)	15(0)	13(1)	12(1)	18(1)	2(1)	5(1)	0(1)
O _D (00)	1857(4)	1184(2)	1930(2)	17(0)	14(1)	23(1)	12(1)	1(1)	4(1)	2(1)
O _D (0z)	1979(3)	1132(2)	6995(2)	16(0)	15(1)	17(1)	12(1)	2(1)	1(1)	2(1)
O _D (m0)	1991(3)	8768(2)	2078(2)	15(0)	12(1)	17(1)	13(1)	0(1)	1(1)	-1(1)
O _D (mz)	1877(4)	8697(2)	7000(2)	18(0)	15(1)	21(1)	15(1)	-2(1)	2(1)	-3(1)
T = 200 °C										
Ca/Sr(0)	2704(1)	10(1)	667(1)	27(0)	11(0)	37(0)	29(0)	0(0)	5(0)	-12(0)
Ca/Sr(z)	2690(1)	59(1)	5640(1)	23(0)	12(0)	29(0)	25(0)	1(0)	6(0)	-4(0)
T ₁ (00)	73(1)	1708(1)	1074(1)	13(0)	14(0)	15(0)	11(0)	-3(0)	7(0)	-1(0)
T ₁ (0z)	31(1)	1746(1)	6155(1)	12(0)	12(0)	13(0)	12(0)	-2(0)	6(0)	0(0)
T ₁ (m0)	21(1)	8197(1)	1173(1)	12(0)	13(0)	14(0)	11(0)	2(0)	6(0)	0(0)
T ₁ (mz)	69(1)	8224(1)	6093(1)	12(0)	13(0)	14(0)	11(0)	3(0)	6(0)	1(0)
T ₂ (00)	6933(1)	1190(1)	1679(1)	12(0)	10(0)	12(0)	13(0)	0(0)	5(0)	0(0)
T ₂ (0z)	6838(1)	1115(1)	6687(1)	12(0)	11(0)	11(0)	14(0)	-1(0)	6(0)	-1(0)
T ₂ (m0)	6852(1)	8854(1)	1748(1)	12(0)	10(0)	11(0)	13(0)	1(0)	4(0)	0(0)
T ₂ (mz)	6936(1)	8782(1)	6724(1)	12(0)	12(1)	11(0)	13(0)	1(0)	6(0)	0(0)
O _A (10)	59(3)	1285(2)	9983(2)	18(0)	23(1)	19(1)	13(1)	-1(1)	10(1)	1(1)
O _A (1z)	9953(3)	1292(2)	4972(2)	18(0)	22(1)	22(1)	12(1)	1(1)	10(1)	2(1)
O _A (20)	5906(3)	9970(2)	1425(2)	17(0)	16(1)	10(1)	25(1)	1(1)	8(1)	2(1)
O _A (2z)	5893(3)	9974(2)	6421(2)	17(0)	11(1)	11(1)	27(1)	-1(1)	5(1)	0(1)
O _B (00)	8265(4)	1205(2)	1024(2)	22(1)	19(1)	25(1)	26(1)	-5(1)	14(1)	-1(1)
O _B (0z)	8069(4)	1207(2)	6076(2)	22(1)	20(1)	24(1)	27(1)	-5(1)	16(1)	1(1)
O _B (m0)	8099(4)	8677(2)	1165(2)	24(1)	18(1)	29(1)	31(1)	5(1)	16(1)	-3(1)
O _B (mz)	8286(4)	8683(2)	6091(2)	22(1)	21(1)	26(1)	27(1)	7(1)	16(1)	3(1)
O _C (00)	142(4)	2933(2)	1232(2)	21(1)	21(1)	18(1)	25(1)	-6(1)	10(1)	-5(1)
O _C (0z)	195(4)	3059(2)	6369(2)	21(1)	19(1)	16(1)	30(1)	-7(1)	11(1)	-6(1)
O _C (m0)	153(3)	6868(2)	1242(2)	20(1)	18(1)	15(1)	25(1)	5(1)	8(1)	2(1)
O _C (mz)	115(4)	6986(2)	6129(2)	21(1)	20(1)	17(1)	25(1)	5(1)	8(1)	2(1)
O _D (00)	1865(4)	1201(2)	1935(2)	24(1)	21(1)	31(1)	16(1)	3(1)	4(1)	2(1)
O _D (0z)	1966(4)	1144(2)	6999(2)	21(1)	18(1)	24(1)	15(1)	2(1)	2(1)	1(1)
O _D (m0)	1987(4)	8775(2)	2071(2)	22(1)	18(1)	26(1)	16(1)	-1(1)	1(1)	-2(1)
O _D (mz)	1879(4)	8704(2)	6991(2)	24(1)	18(1)	29(1)	17(1)	-1(1)	2(1)	-3(1)

continued on next page

tetrahedra reported in Table 7 indicate that the topochemical symmetry of the framework of $\text{An}_{20}\text{SrF}_{80}$ feldspar is essentially monoclinic. The average dimensions of the (00) and (mz) pseudo-symmetrical tetrahedra and of the (0z) and (m0) pseudo-symmetrical tetrahedra do not change within the error limits. The macroscopic Al,Si order parameter Q_{ods} , calculated from the room temperature data using the calibration by Angel et al. (1990), is 0.88.

The structure of $\text{An}_{20}\text{SrF}_{80}$ at high-temperature

The edge dimensions of the unit-cell of $\text{An}_{20}\text{SrF}_{80}$ feldspar vary linearly with temperature (Table 3, Fig. 4). The most significant expansion is observed in a and c , while b is almost constant. With increasing temperature, the α and γ angles

progressively approach 90°. McGuinn and Redfern (1997) observed strain-tails in α and in γ close to the critical temperature (T_c) of the $I2/c$ - $I\bar{1}$ transition, and interpreted these tails in terms of inhomogeneity of the M cation distribution, related to tweed microstructures noted in previous investigations. The data collected in this work were not sufficiently detailed to see this effect. On the basis of the cell-dimension variations presented here, the observed temperature of the transition (T_w) is ~ 520 °C.

According to McGuinn and Redfern (1997), the e_4 strain component behaves as the primary order parameter for the $I\bar{1}$ - $I2/c$ transition. Because e_4 can be approximated as $\approx -\cos \alpha^*$ (Salje et al. 1985), and because (for a second-order transition) the order parameter Q is related to the spontaneous strain ε according to $\varepsilon^2 \propto Q^2 \propto T$ (Carpenter 1988), it is therefore ex-

TABLE 5.—Continued

Site	x	y	z	U_{eq}	U_{11}	U_{22}	U_{33}	U_{12}	U_{13}	U_{23}
$T = 400 \text{ }^{\circ}\text{C}$										
Ca/Sr(0)	2713(1)	-2(1)	665(1)	34(0)	17(0)	45(0)	37(0)	0(0)	8(0)	-11(0)
Ca/Sr(z)	2702(1)	41(1)	5650(1)	31(0)	17(0)	40(0)	34(0)	1(0)	9(0)	-1(0)
T ₁ (00)	74(2)	1725(1)	1079(1)	16(0)	17(1)	19(1)	15(1)	-3(0)	9(0)	-1(0)
T ₁ (0z)	27(2)	1762(1)	6158(1)	16(0)	19(1)	16(1)	17(1)	-3(0)	10(1)	-1(0)
T ₁ (m0)	24(2)	8205(1)	1168(1)	16(0)	19(1)	18(1)	15(1)	4(0)	10(1)	1(0)
T ₁ (mz)	73(2)	8234(1)	6090(1)	16(0)	17(1)	18(1)	15(1)	4(0)	9(1)	0(0)
T ₂ (00)	6945(2)	1197(1)	1691(1)	16(0)	15(1)	16(1)	18(1)	-1(0)	8(1)	0(0)
T ₂ (0z)	6846(2)	1123(1)	6700(1)	15(0)	14(1)	13(0)	18(1)	-1(0)	7(1)	-1(0)
T ₂ (m0)	6862(2)	8860(1)	1740(1)	16(0)	16(1)	13(0)	18(1)	2(0)	7(1)	0(0)
T ₂ (mz)	6942(2)	8786(1)	6717(1)	16(0)	16(1)	15(1)	18(1)	1(0)	9(1)	0(0)
O _A (10)	54(5)	1292(3)	9994(2)	24(1)	31(2)	26(2)	18(2)	0(1)	14(2)	-1(1)
O _A (1z)	9950(5)	1298(3)	4979(2)	25(1)	33(2)	29(2)	17(2)	2(1)	16(2)	2(1)
O _A (20)	5920(4)	9983(2)	1431(3)	24(1)	20(2)	14(1)	36(2)	2(1)	9(2)	3(1)
O _A (2z)	5913(4)	9985(2)	6426(3)	24(1)	19(2)	14(1)	36(2)	0(1)	10(2)	0(1)
O _B (00)	8278(5)	1237(3)	1039(3)	29(1)	25(2)	35(2)	33(2)	-9(1)	20(2)	-4(1)
O _B (0z)	8079(5)	1241(3)	6097(3)	31(1)	27(2)	34(2)	41(2)	-5(1)	24(2)	2(2)
O _B (m0)	8100(5)	8896(3)	1149(3)	34(1)	29(2)	40(2)	43(2)	8(2)	26(2)	-2(2)
O _B (mz)	8292(5)	8700(3)	6080(3)	29(1)	25(2)	35(2)	35(2)	8(1)	21(2)	3(2)
O _C (00)	147(5)	2953(3)	1212(3)	30(1)	33(2)	19(2)	38(2)	-8(1)	15(2)	-5(1)
O _C (0z)	188(5)	3080(3)	6340(3)	28(1)	25(2)	20(2)	38(2)	-8(1)	14(2)	-5(1)
O _C (m0)	172(5)	6879(3)	1274(3)	28(1)	24(2)	21(2)	35(2)	8(1)	9(2)	2(1)
O _C (mz)	127(5)	7001(3)	6150(3)	29(1)	32(2)	19(1)	35(2)	8(1)	13(2)	4(1)
O _D (00)	1863(5)	1221(3)	1943(3)	32(1)	28(2)	41(2)	24(2)	6(2)	8(2)	4(2)
O _D (0z)	1966(5)	1161(3)	7012(3)	29(1)	30(2)	31(2)	20(2)	4(1)	4(2)	3(1)
O _D (m0)	1977(5)	8794(3)	2058(3)	30(1)	25(2)	34(2)	24(2)	-1(1)	4(2)	-4(1)
O _D (mz)	1877(5)	8717(3)	6979(3)	32(1)	28(2)	42(2)	20(2)	-1(2)	4(2)	-5(1)
$T = 500 \text{ }^{\circ}\text{C}$										
Ca/Sr(0)	2715(1)	-17(1)	661(1)	37(0)	19(0)	46(0)	43(0)	-1(0)	11(0)	-7(0)
Ca/Sr(z)	2714(1)	24(1)	5660(1)	37(0)	20(0)	46(0)	42(0)	-1(0)	11(0)	1(0)
T ₁ (00)	73(2)	1746(1)	1082(1)	19(0)	20(1)	20(1)	21(1)	-5(0)	12(1)	-3(0)
T ₁ (0z)	27(2)	1777(1)	6163(1)	19(0)	18(1)	20(1)	21(1)	-4(1)	11(1)	-2(1)
T ₁ (m0)	25(2)	8218(1)	1166(1)	19(0)	20(1)	19(1)	21(1)	3(1)	12(1)	0(1)
T ₁ (mz)	75(2)	8250(1)	6085(1)	19(0)	18(1)	21(1)	19(1)	3(0)	10(1)	-1(0)
T ₂ (00)	6950(2)	1207(1)	1706(1)	18(0)	16(1)	18(1)	22(1)	-2(1)	9(1)	-2(1)
T ₂ (0z)	6853(2)	1130(1)	6719(1)	18(0)	17(1)	14(1)	25(1)	-3(0)	10(1)	-3(0)
T ₂ (m0)	6858(2)	8867(1)	1724(1)	18(0)	17(1)	15(1)	24(1)	1(0)	10(1)	-1(0)
T ₂ (mz)	6948(2)	8792(1)	6707(1)	18(0)	17(1)	17(1)	23(1)	-1(1)	10(1)	-2(1)
O _A (10)	47(5)	1294(3)	4(3)	27(1)	36(2)	31(2)	19(2)	-1(2)	17(2)	-4(1)
O _A (1z)	9950(5)	1296(3)	4992(3)	28(1)	35(2)	31(2)	21(2)	2(2)	16(2)	1(1)
O _A (20)	5919(5)	2(3)	1423(3)	28(1)	23(2)	15(1)	45(2)	0(1)	14(2)	-1(1)
O _A (2z)	5917(5)	0(2)	6425(3)	27(1)	19(2)	14(1)	45(2)	-3(1)	11(2)	-3(1)
O _B (00)	8295(6)	1261(3)	1062(4)	35(1)	29(2)	39(2)	45(2)	-9(2)	25(2)	-5(2)
O _B (0z)	8092(6)	1267(3)	6117(4)	36(1)	29(2)	40(2)	51(3)	-8(2)	27(2)	1(2)
O _B (m0)	8094(6)	8723(3)	1130(4)	37(1)	31(2)	39(2)	50(3)	11(2)	26(2)	-4(2)
O _B (mz)	8291(6)	8730(3)	6065(4)	36(1)	34(2)	40(2)	49(3)	11(2)	32(2)	1(2)
O _C (00)	136(6)	2972(3)	1190(3)	33(1)	31(2)	23(2)	43(2)	-8(2)	14(2)	-6(2)
O _C (0z)	189(5)	3096(3)	6317(3)	32(1)	29(2)	23(2)	45(2)	-8(1)	16(2)	-7(2)
O _C (m0)	174(5)	6896(3)	1302(3)	32(1)	28(2)	22(2)	47(2)	5(1)	17(2)	2(2)
O _C (mz)	132(6)	7020(3)	6176(3)	34(1)	33(2)	25(2)	41(2)	7(2)	15(2)	4(2)
O _D (00)	1870(6)	1246(3)	1958(3)	38(1)	37(3)	45(2)	28(2)	5(2)	10(2)	4(2)
O _D (0z)	1965(6)	1187(3)	7026(3)	34(1)	26(2)	41(2)	24(2)	-1(2)	2(2)	0(2)
O _D (m0)	1974(6)	8803(3)	2038(3)	34(1)	32(2)	38(2)	25(2)	-4(2)	5(2)	-7(2)
O _D (mz)	1867(6)	8743(3)	6960(3)	36(1)	27(2)	48(2)	25(2)	-3(2)	3(2)	-8(2)
$T = 620 \text{ }^{\circ}\text{C}$										
Ca/Sr	2723(1)	-19(1)	661(1)	41(0)	22(0)	55(0)	43(0)	0(0)	9(0)	-4(0)
T ₁ (0)	70(1)	1752(1)	1082(1)	20(0)	21(0)	25(0)	17(0)	-4(0)	10(0)	-1(0)
T ₁ (z)	30(1)	1781(1)	6165(1)	20(0)	22(1)	23(0)	18(0)	-4(0)	10(0)	-1(0)
T ₂ (0)	6955(1)	1209(1)	1708(1)	20(0)	19(0)	20(0)	21(0)	-1(0)	8(0)	0(0)
T ₂ (z)	6863(1)	1133(1)	6722(1)	19(0)	18(0)	18(0)	22(0)	-2(0)	8(0)	-1(0)
O _A (1)	53(3)	1303(2)	5(2)	30(0)	39(1)	36(1)	18(1)	-1(1)	16(1)	-2(1)
O _A (2)	5930(3)	2(2)	1426(2)	30(0)	23(1)	19(1)	44(1)	1(1)	10(1)	1(1)
O _B (0)	8290(4)	1273(2)	1062(2)	38(1)	32(1)	45(2)	45(2)	-12(1)	25(1)	-5(1)
O _B (z)	8098(4)	1276(2)	6125(2)	40(1)	30(1)	50(2)	51(2)	-7(1)	27(1)	5(1)
O _C (0)	137(4)	2985(2)	1180(2)	37(1)	35(2)	28(1)	43(1)	-10(1)	13(1)	-7(1)
O _C (z)	198(3)	3100(2)	6311(2)	35(1)	30(1)	26(1)	48(1)	-11(1)	16(1)	-6(1)
O _D (0)	1865(4)	1252(3)	1957(2)	42(1)	35(2)	55(2)	24(1)	5(1)	3(1)	5(1)
O _D (z)	1979(4)	1190(2)	7038(2)	39(1)	35(2)	43(2)	27(1)	3(1)	4(1)	2(1)

Notes: U_{eq} defined as one third of the trace of the orthogonalized U_i tensor. The anisotropic displacement exponent takes the form: $-2\pi^2 (\beta^2 U_{11} + k^2 b^2 U_{22} + l^2 c^2 U_{33} + 2hka^2 b^2 U_{12} + 2ila^2 c^2 U_{13} + 2kb^2 c^2 U_{23})$.

TABLE 6. Ca/Sr-O bond lengths (\AA)

T (°C)	20	200	400	500	620	
Space group	$/\bar{1}$	$/\bar{1}$	$/\bar{1}$	$/\bar{1}$	$/\bar{1}$	$/2/c$
Ca/Sr(0)-O _A (10)	2.598(2)	2.614(3)	2.632(4)	2.642(4)		
Ca/Sr(0)-O _A (10)	2.650(2)	2.659(3)	2.667(4)	2.663(4)		
Ca/Sr(0)-O _A (20)	2.410(2)	2.420(3)	2.426(4)	2.424(4)		
Ca/Sr(0)-O _B (00)	2.654(3)	2.675(3)	2.712(4)	2.750(4)		
Ca/Sr(0)-O _B (m0)	2.979(3)	2.965(3)	2.933(4)	2.889(5)		
Ca/Sr(0)-O _C (0z)	3.204(3)	3.179(3)	3.129(4)	3.084(4)		
Ca/Sr(0)-O _C (mz)	3.110(2)	3.129(3)	3.167(4)	3.213(4)		
Ca/Sr(0)-O _D (00)	2.657(3)	2.684(3)	2.726(4)	2.780(5)	Ca/Sr-O _A (1)	2.651(3)
Ca/Sr(0)-O _D (m0)	2.844(2)	2.834(3)	2.805(4)	2.766(4)	Ca/Sr-O _A (1)	2.682(3)
< [6] M(0)-O>	2.635	2.648	2.661	—	Ca/Sr-O _A (2)	2.430(3)
< [7] M(0)-O>	2.684	2.693	2.700	2.702	Ca/Sr-O _B (0)	2.762(3)
< [9] M(0)-O>	2.789	2.795	2.800	2.801	Ca/Sr-O _B (z)	2.879(3)
					Ca/Sr-O _C (0)	3.212(3)
Ca/Sr(z)-O _A (1z)	2.619(2)	2.633(3)	2.641(4)	2.642(4)	Ca/Sr-O _C (z)	3.078(3)
Ca/Sr(z)-O _A (1z)	2.627(2)	2.636(3)	2.656(4)	2.667(4)	Ca/Sr-O _D (0)	2.795(3)
Ca/Sr(z)-O _A (2z)	2.418(2)	2.424(2)	2.430(4)	2.424(4)	Ca/Sr-O _D (z)	2.761(3)
Ca/Sr(z)-O _B (0z)	2.739(2)	2.764(3)	2.817(4)	2.864(5)	< [7] M-O>	2.708
Ca/Sr(z)-O _B (mz)	2.776(2)	2.794(3)	2.787(4)	2.761(4)	< [9] M-O>	2.805
Ca/Sr(z)-O _C (00)	3.380(3)	3.346(3)	3.294(4)	3.236(4)		
Ca/Sr(z)-O _C (m0)	2.953(3)	2.971(3)	3.015(4)	3.056(4)		
Ca/Sr(z)-O _D (0z)	2.637(3)	2.659(3)	2.696(4)	2.742(4)		
Ca/Sr(z)-O _D (mz)	2.940(3)	2.907(3)	2.862(4)	2.802(5)		
< [6] M(z)-O>	2.636	2.652	—	—		
< [7] M(z)-O>	2.679	2.688	2.698	2.700		
< [9] M(z)-O>	2.788	2.793	2.800	2.799		

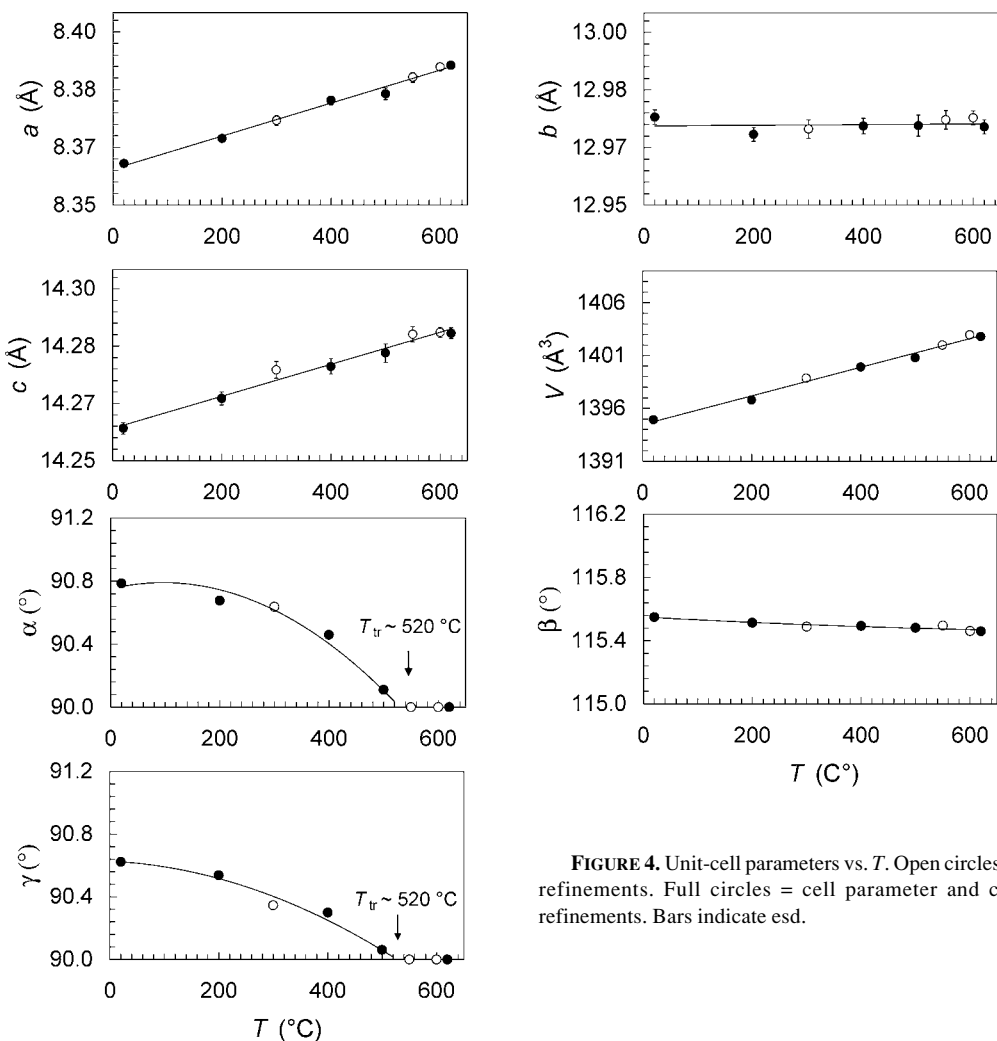
**FIGURE 4.** Unit-cell parameters vs. T . Open circles = cell parameter refinements. Full circles = cell parameter and crystal structure refinements. Bars indicate esd.

TABLE 7. T-O bond lengths (\AA)

T ($^{\circ}\text{C}$)	20	200	400	500	620	
Space group	/ $\bar{1}$	$I2/c$				
$T_1(00)$ - $O_A(10)$	1.643(2)	1.639(2)	1.637(3)	1.637(3)		
$T_1(00)$ - $O_B(00)$	1.618(3)	1.614(3)	1.608(4)	1.604(4)		
$T_1(00)$ - $O_C(00)$	1.602(3)	1.599(3)	1.600(4)	1.597(4)		
$T_1(00)$ - $O_D(00)$	1.625(3)	1.625(3)	1.621(4)	1.623(5)	$T_1(0)$ - $O_A(1)$	1.639(2)
Mean	1.622	1.619	1.616	1.615	$T_1(0)$ - $O_B(0)$	1.606(3)
$T_1(mz)$ - $O_A(1z)$	1.646(2)	1.642(2)	1.639(3)	1.639(4)	$T_1(0)$ - $O_C(0)$	1.604(3)
$T_1(mz)$ - $O_B(mz)$	1.613(3)	1.610(3)	1.607(4)	1.609(4)	$T_1(0)$ - $O_D(0)$	1.622(3)
$T_1(mz)$ - $O_C(mz)$	1.613(2)	1.608(3)	1.603(4)	1.600(4)	Mean	1.618
$T_1(mz)$ - $O_D(mz)$	1.615(3)	1.617(3)	1.616(4)	1.615(4)		
Mean	1.622	1.619	1.616	1.616		
$T_1(0z)$ - $O_A(1z)$	1.756(2)	1.755(2)	1.758(3)	1.757(4)		
$T_1(0z)$ - $O_B(0z)$	1.736(3)	1.736(3)	1.730(4)	1.725(4)	$T_1(z)$ - $O_A(1)$	1.755(2)
$T_1(0z)$ - $O_C(0z)$	1.719(3)	1.720(3)	1.722(4)	1.723(4)	$T_1(z)$ - $O_B(z)$	1.726(3)
$T_1(0z)$ - $O_D(0z)$	1.754(3)	1.746(3)	1.748(4)	1.740(4)	$T_1(z)$ - $O_C(z)$	1.721(3)
Mean	1.741	1.739	1.740	1.736	$T_1(z)$ - $O_D(z)$	1.750(3)
Mean	1.741	1.741	1.741	1.740	Mean	1.738
$T_1(00)$ - $O_A(20)$	1.752(2)	1.750(2)	1.749(3)	1.745(4)		
$T_1(00)$ - $O_B(00)$	1.737(3)	1.736(3)	1.734(4)	1.736(4)	$T_2(0)$ - $O_A(2)$	1.748(2)
$T_1(00)$ - $O_C(mz)$	1.740(3)	1.737(3)	1.738(4)	1.738(4)	$T_2(0)$ - $O_B(0)$	1.731(3)
$T_1(00)$ - $O_D(mz)$	1.727(3)	1.725(3)	1.724(4)	1.729(4)	$T_2(0)$ - $O_C(0)$	1.732(3)
Mean	1.739	1.737	1.736	1.737	$T_2(0)$ - $O_D(0)$	1.731(3)
$T_2(mz)$ - $O_A(2z)$	1.747(2)	1.748(2)	1.746(3)	1.752(4)	$T_2(z)$ - $O_A(2)$	1.748(2)
$T_2(mz)$ - $O_B(mz)$	1.732(3)	1.728(3)	1.733(4)	1.732(4)	$T_2(z)$ - $O_B(0)$	1.731(3)
$T_2(mz)$ - $O_C(00)$	1.727(3)	1.733(3)	1.728(4)	1.735(4)	$T_2(z)$ - $O_C(0)$	1.732(3)
$T_2(mz)$ - $O_D(00)$	1.742(3)	1.735(3)	1.736(4)	1.730(5)	Mean	1.736
Mean	1.737	1.736	1.736	1.737		
$T_2(0z)$ - $O_A(2z)$	1.638(2)	1.632(2)	1.631(3)	1.629(4)		
$T_2(0z)$ - $O_B(0z)$	1.618(3)	1.615(3)	1.611(4)	1.617(4)		
$T_2(0z)$ - $O_C(m0)$	1.619(3)	1.617(3)	1.609(4)	1.615(4)		
$T_2(0z)$ - $O_D(m0)$	1.617(3)	1.618(3)	1.618(4)	1.620(4)	$T_2(z)$ - $O_A(2)$	1.634(2)
Mean	1.623	1.620	1.617	1.620	$T_2(z)$ - $O_B(z)$	1.610(3)
$T_2(z)$ - $O_A(20)$	1.633(2)	1.631(2)	1.631(3)	1.638(4)	$T_2(z)$ - $O_D(z)$	1.615(3)
$T_2(z)$ - $O_B(m0)$	1.609(3)	1.607(3)	1.609(4)	1.607(4)	Mean	1.617
$T_2(z)$ - $O_C(0z)$	1.612(3)	1.610(3)	1.614(4)	1.608(4)		
$T_2(z)$ - $O_D(0z)$	1.624(3)	1.628(3)	1.622(4)	1.628(4)		
Mean	1.619	1.619	1.619	1.620		

Note: Bond lengths were not corrected for vibrational motion.

pected that $\cos^2\alpha^* \propto T$. The variation of $\cos^2\alpha^*$ with temperature (Fig. 5) is consistent with the solution to Landau 2-4-6 potential with $T_c = 506 \pm 7$ $^{\circ}\text{C}$. This temperature is significantly lower than that obtained by McGuinn and Redfern (1997) ($T_c = 680$ $^{\circ}\text{C}$), but is in agreement with the values determinated by Nager et al. (1970) and Tribaudino et al. (1993).

In order to evaluate the “monoclinic” intensity distribution, the R^* factor for all the observed pairs F hkl and F $h\bar{k}l$, was calculated according to Winter et al. (1979). These R^* values obtained at different temperatures are reported in Table 4. They decrease with increasing temperature, reaching a value close to monoclinic symmetry at $T = 500$ $^{\circ}\text{C}$. At $T = 620$ $^{\circ}\text{C}$, the significantly small R^* value (triclinic refinement) indicates the achievement of monoclinic symmetry within average fluctuations of Fo due to counting errors.

The “obliquity” for $\text{An}_{20}\text{SrF}_{80}$ feldspar is reported in Table 8. This is a monoclinic indicator based on atomic position (Winter et al. 1979). The “obliquity” values (Δx , Δy , and Δz)

give a direct measure of deviations from monoclinic symmetry at the atomic level. The trend of the Δ values to zero with increasing temperature also indicates convergence to the monoclinic symmetry at high temperatures. In Figure 6, the “obliquity” values are plotted against $\cos \alpha^*$. To simplify the figure, only the values calculated for the OB and OD atoms are reported, as they have larger displacements. The figure shows that the local atomic displacements scale with the order parameter.

With increasing temperature, the non-tetrahedral cation polyhedron progressively modifies. At high temperature, the changes occurring in the $\text{Ca/Sr}(0)$ and $\text{Ca/Sr}(z)$ polyhedra are dominated by the progressive tendency toward monoclinic symmetry (Table 6). Figure 7 shows that the distances between the M cation and the pseudo-related O atom pairs converge on the values adopted at the $\bar{1}/I2/c$ transition, when the pseudo-related atom pairs become equivalent. The Ca/Sr -polyhedron assumes an even more regular coordination (Fig. 2c), practically identical to that observed in monoclinic Sr feldspar at

TABLE 8. "Obliquity" ($\times 10^3$) as a function of temperature

T (°C)	20			200			400			500			620*		
	Δx	Δy	Δz	Δx	Δy	Δz	Δx	Δy	Δz	Δx	Δy	Δz	Δx	Δy	Δz
Ca/Sr	1.6	8.6	3.9	1.5	6.8	2.7	1.1	3.9	1.5	0.1	0.7	0.1	0.0	0.3	0.0
$T_1(0)$	0.2	8.1	2.4	0.4	6.8	1.8	0.1	4.1	1.2	-0.2	0.5	0.2	0.1	0.2	-0.1
$T_1(z)$	0.7	6.9	2.2	1.0	5.7	1.9	0.4	3.3	1.0	0.2	0.5	0.4	0.1	-0.1	0.1
$T_2(0)$	0.8	3.4	5.6	0.3	2.8	4.5	-0.4	1.6	2.6	-0.2	0.1	0.1	-0.2	-0.1	0.1
$T_2(z)$	1.4	3.6	7.3	1.4	3.1	6.1	1.6	1.7	4.1	0.4	0.4	0.5	0.0	-0.1	0.1
$O_A(1)$	0.9	0.8	5.6	1.2	0.7	4.5	0.3	0.6	2.8	-0.3	0.3	0.3	-0.7	0.2	-0.2
$O_A(2)$	1.0	6.8	0.1	1.3	5.6	-0.3	0.7	3.3	-0.5	0.3	-0.1	0.2	-0.5	-0.1	0.4
$O_B(0)$	2.4	13.2	7.4	2.0	11.3	6.7	1.5	6.3	4.1	-0.4	0.8	0.3	0.3	-0.4	0.2
$O_B(z)$	3.8	13.1	10.7	3.0	11.5	8.8	2.1	6.3	5.1	0.2	1.0	1.3	-0.5	-0.7	-0.1
$O_C(0)$	5.3	9.7	12.3	2.8	8.1	10.3	2.0	4.6	6.2	0.4	0.8	1.4	-0.1	0.1	0.5
$O_C(z)$	4.9	8.8	15.2	4.2	7.4	12.7	1.6	4.2	6.6	1.5	0.8	1.4	0.6	-0.3	0.7
$O_D(0)$	2.0	11.9	7.0	1.3	9.5	5.6	1.4	6.2	3.7	-0.3	1.1	0.3	-0.2	0.6	0.4
$O_D(z)$	1.3	10.0	8.3	2.1	8.2	7.2	1.1	4.5	4.6	0.9	1.0	1.2	-0.4	0.4	0.3

Notes: Δx , Δy and Δz are the differences (in absolute value) in the coordinates of atom pairs related by the pseudo \mathcal{D}/c symmetry. A negative value indicates that the calculated value has passed through zero with increasing temperature (according to Winter et al. 1979).

* Triclinic model.

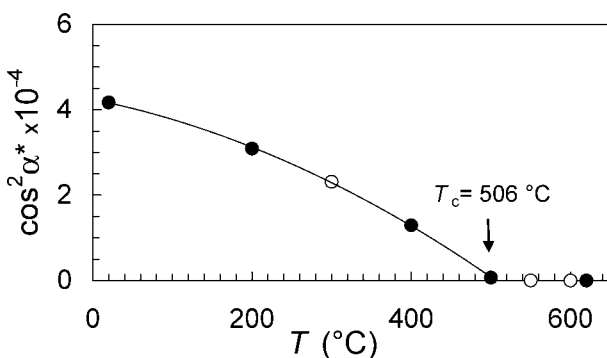


FIGURE 5. Variation of $\cos^2 \alpha^*$ ($\approx Q^2$) vs. T . At $T_c = 506 \pm 7$ °C, $\cos^2 \alpha^*$ goes to zero. Symbols as in Figure 4.

room temperature. In addition to the modification observed in the M-O distances, as temperature is raised, the values of the T-O_B-T and T-O_D-T angles, relative to the pseudo-related O atom pairs (which are already different at room temperature), converge on the values adopted at the transition temperature (Fig. 8). The T-O-T angles at T_{tr} are similar to those observed in monoclinic Sr feldspar at room temperature. The results obtained indicate $T_{tr} \sim 520$ °C, in agreement with the transition temperature obtained from the variations of cell dimensions.

The average T-O bond lengths, and therefore the Al,Si site occupancies, are not significantly changed at high-temperature (Table 7). Therefore, the Al-Si distribution remains nearly unchanged throughout the investigated temperature range.

In Figure 9, the evolution with temperature of the isotropic equivalent displacement parameters (B_{eq}) is plotted for an average of M, O, and T atoms respectively. Extrapolations of the higher temperature data to 0 K show the presence of some residual. The residual is higher for the non-tetrahedral cation and can be ascribed to the partial Ca-Sr substitution.

In conclusion, in $\text{An}_{20}\text{SrF}_{80}$ feldspar at room temperature, partial Ca-Sr substitution and the consequent decrease of the mean ionic radius of the non-tetrahedral cation causes the collapse from monoclinic symmetry of Sr feldspar to triclinic symmetry. Changes observed at room temperature highlight the progressive modification of the M-polyhedron along the SrF-

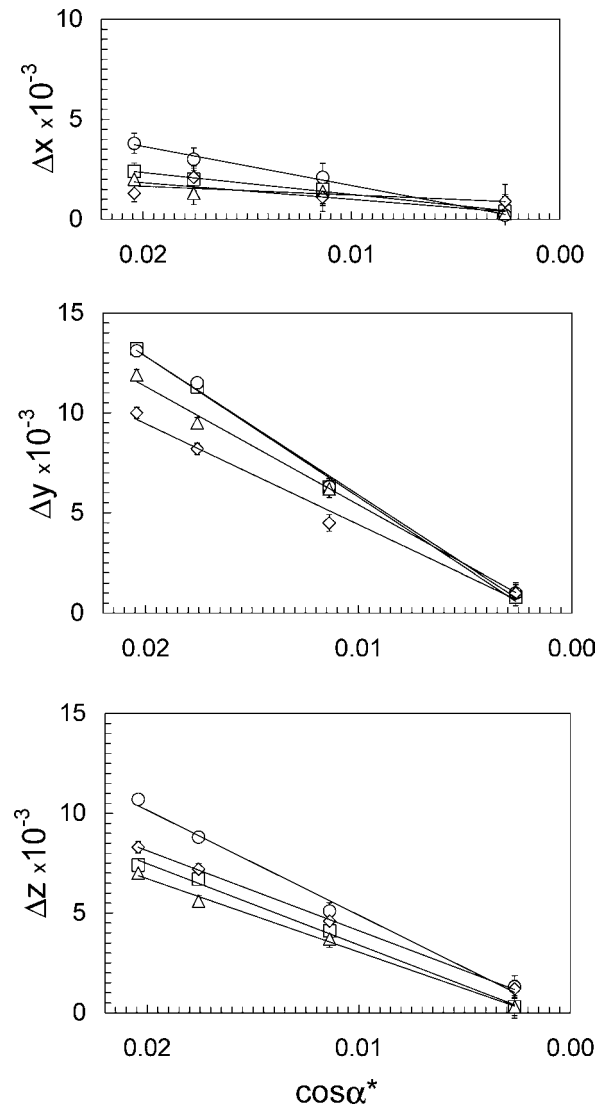


FIGURE 6. Δx , Δy , and Δz (see Table 8) calculated for OB and OD atoms vs. $\cos \alpha^*$. Squares = $O_B(0)$; circles = $O_B(z)$; triangles = $O_D(0)$; diamonds = $O_D(z)$. Bars indicate estimated errors.

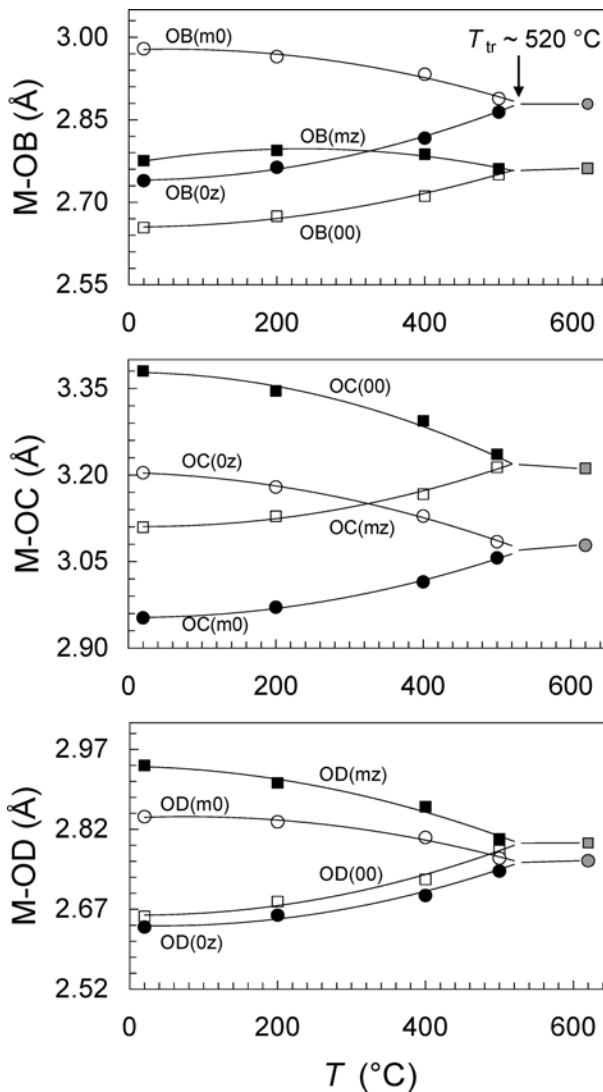


FIGURE 7. M-O distances vs. T . Squares: (00) and (mz) pseudo-related O atom pairs; circles: (0z) and (m0). Open symbol: Ca/Sr(0)-polyhedron; full symbol: Ca/Sr(z)-polyhedron; grey symbol: $I2/c$ configuration.

An join toward the configuration observed in the Ca-polyhedron in anorthite. With increasing temperature, the unit-cell parameter variations, the intensities of $h k l$ and $h \bar{k} l$ reflections, and the Ca/Sr-O distances, all converge toward monoclinic symmetry with an observed transition temperature of 520 ± 10 °C, whereas T_c , as indicated from the Landau 2-4-6 expansion, is 506 ± 7 °C. At transition, the structure of $\text{An}_{20}\text{SrF}_{80}$ feldspar is similar to that of monoclinic Sr feldspar at room temperature. In ordered $\text{An}_{20}\text{SrF}_{80}$ feldspar ($Q_{od} = 0.88$), no discontinuities are detectable in the Ca/Sr-O bond length variations with temperature according to the continuous character of the $I\bar{I}-I2/c$ transition.

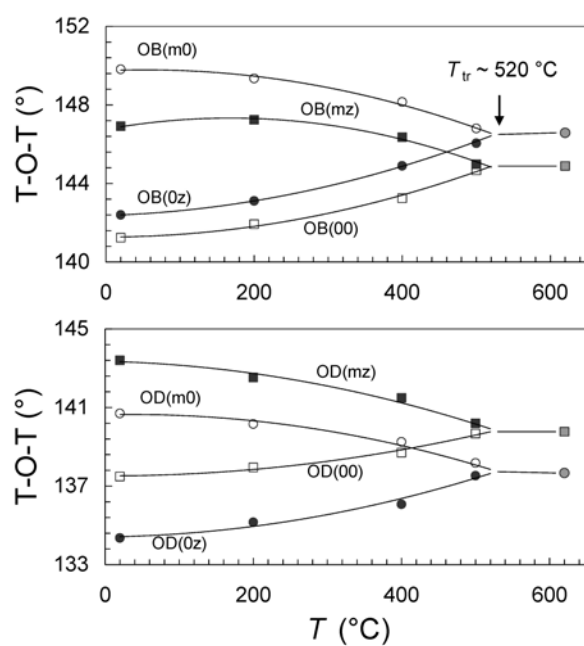


FIGURE 8. T-O_B-T and T-O_D-T angles vs. T . Symbols as in Figure 7.

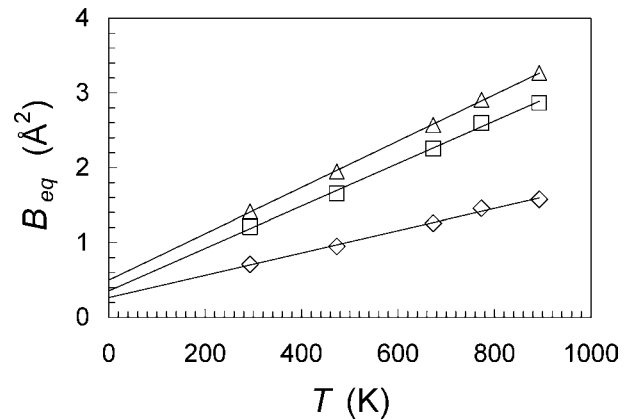


FIGURE 9. Equivalent isotropic displacement factors B_{eq} vs. T . Triangles = Ca/Sr atom. Squares = O atoms. Diamonds = T atoms.

ACKNOWLEDGMENTS

Reviews from Michael A. Carpenter and Simon A.T. Redfern greatly improved the manuscript; we thank them for critical reading and helpful suggestions. This work was supported by Project “Structural Evolution and Phase Transitions in Minerals versus Temperature, Pressure, and Composition” (MURST, Roma) and by Istituto di Geoscienze e Georisorse (CNR, Torino).

REFERENCES CITED

- Angel, R.J., Carpenter, M.A., and Finger, L.W. (1990) Structural variation associated with compositional variation and order-disorder behavior in anorthite-rich feldspar. American Mineralogist, 75, 150–162.
- Bambauer, H.U. and Nager, H.E. (1981) Gitterkonstanten und displazive Transformationen synthetischer Erdalkalifeldspäte. I. System $\text{Ca}[\text{Al}_2\text{Si}_2\text{O}_8]-\text{Sr}[\text{Al}_2\text{Si}_2\text{O}_8]-\text{Ba}[\text{Al}_2\text{Si}_2\text{O}_8]$. Neues Jahrbuch für Mineralogie Abhandlungen, 141, 225–239.

- Benna, P. and Bruno, E. (2001) Single-crystal in situ high-temperature structural investigation on strontium feldspar. *American Mineralogist*, 86, 690–696.
- Benna, P., Tribaudino, M., and Bruno, E. (1995) Al-Si ordering in Sr-feldspar $\text{SrAl}_2\text{Si}_2\text{O}_8$: IR, TEM and single-crystal XRD evidences. *Physics and Chemistry of Minerals*, 22, 343–350.
- (1996) The structure of ordered and disordered lead feldspar ($\text{PbAl}_2\text{Si}_2\text{O}_8$). *American Mineralogist*, 81, 1337–1343.
- Biggar, G.M. and O'Hara, M.J. (1969) A comparison of gel and glass starting materials for phase equilibrium studies. *Mineralogical Magazine*, 36, 198–205.
- Bruno, E. and Facchinelli, A. (1974) Correlations between the unit-cell dimensions and the chemical and structural parameters in plagioclases and in alkaline-earth feldspars. *Bulletin de la Société française de Minéralogie et de Cristallographie*, 97, 378–385.
- Bruno, E. and Gazzoni, G. (1968) Feldspati sintetici della serie $\text{CaAl}_2\text{Si}_2\text{O}_8\text{-SrAl}_2\text{Si}_2\text{O}_8$. *Atti dell'Accademia delle Scienze di Torino*, 102, 881–893.
- Carpenter, M.A. (1988) Thermochemistry of aluminium/silicon ordering in feldspar minerals. In E.K.H. Salje, Ed., *Physical properties and thermodynamic behaviour of minerals*, NATO ASI series C/225, p. 265–323. Reidel Publishing Company, Dordrecht, Holland.
- Chiari, G., Calleri, M., Bruno, E., and Ribbe, P.H. (1975) The structure of partially disordered, synthetic strontium feldspar. *American Mineralogist*, 60, 111–119.
- Chiari, G., Facchinelli, A., and Bruno, E. (1978) Anorthite quenched from 1530 °C. II. Discussion. *Acta Crystallographica*, B34, 17571–1764.
- Czank, M. (1973) Strukturuntersuchungen von Anorthit im Temperaturbereich von 20 °C bis 1430 °C. Dissertation. ETH Zürich.
- Dove, M.T. and Redfern, S.A.T. (1997) Lattice simulation studies of the ferroelastic phase transitions in disordered $(\text{Na}, \text{K})\text{AlSi}_3\text{O}_8$ and ordered $(\text{Sr}, \text{Ca})\text{Al}_2\text{Si}_2\text{O}_8$ feldspar solid solutions. *American Mineralogist*, 82, 8–15.
- Foit, F.F. and Peacor, J.R. (1973) The anorthite crystal structure at 410 and 830 °C. *American Mineralogist*, 58, 665–675.
- Kalus, C. (1978) Neue Strukturbestimmung des Anorthits unter Berücksichtigung möglicher Alternativen. Inaugural-Dissertation, Universität München.
- Kroll, H. and Müller, W.F. (1980) X-ray and electron-optical investigation of synthetic high-temperature plagioclases. *Physics and Chemistry of Minerals*, 5, 255–277.
- McGuinn, M.D. and Redfern, S.A.T. (1994) Ferroelastic phase transition along the join $\text{CaAl}_2\text{Si}_2\text{O}_8\text{-SrAl}_2\text{Si}_2\text{O}_8$. *American Mineralogist*, 79, 24–30.
- (1997) High-temperature ferroelastic strain below the $\text{I}2/\text{c} - \text{I}\bar{1}$ transition in $\text{Ca}_{1-x}\text{Sr}_x\text{Al}_2\text{Si}_2\text{O}_8$ feldspars. *European Journal of Mineralogy*, 9, 1159–1172.
- Megaw, H.D. (1974) Tilts and tetrahedra in feldspars. In W.S. MacKenzie and J. Zussman, Eds., *The feldspars*, p. 87–113. Manchester University Press, Manchester.
- Megaw, H.D., Kempster, C.J.E., and Radoslovich, E.W. (1962) The structure of anorthite $\text{CaAl}_2\text{Si}_2\text{O}_8$. II. Description and discussion. *Acta Crystallographica*, 15, 1017–1035.
- Nager, H.E. (1969) *Strontiumfeldspat und die Mischreihe $(\text{Sr}, \text{Ca})[\text{Al}_2\text{Si}_2\text{O}_8]$* . Diplomarbeit, University of Münster.
- Nager, H.E., Hoffmann, W., and Nissen, H.U. (1969) Die Mischreihe $(\text{Ca}, \text{Sr})[\text{Al}_2\text{Si}_2\text{O}_8]$. *Naturwissenschaften*, 56, 136.
- Nager, H.E., Bambauer, H.U., and Hoffmann, W. (1970) Polymorphie in der Mischreihe $(\text{Ca}, \text{Sr})[\text{Al}_2\text{Si}_2\text{O}_8]$. *Naturwissenschaften*, 57, 86–87.
- North, A.C.T., Phillips, D.C., and Mathews, F.S. (1968) A semi-empirical method of absorption correction. *Acta Crystallographica*, A24, 351–359.
- Phillips, B.L., McGuinn, M.D., and Redfern, S.A.T. (1997) Si-Al order and the $\text{I}\bar{1}/\text{c}$ structural phase transition in synthetic $\text{CaAl}_2\text{Si}_2\text{O}_8\text{-SrAl}_2\text{Si}_2\text{O}_8$ feldspar: A ^{29}Si MAS-NMR spectroscopy study. *American Mineralogist*, 82, 1–7.
- Salje, E., Kuscholke, B., Wruck, B., and Kroll, H. (1985) Thermodynamics of sodium feldspar II: Experimental results and numerical calculations. *Physics and Chemistry of Minerals*, 12, 99–107.
- Sheldrick, G.M. (1997) *SHELXL-97-A* program for crystal structure refinement. University of Goettingen, Germany. Release 97–2.
- Tribaudino, M., Benna, P., and Bruno, E. (1993) $\text{I}\bar{1}$ - $\text{I}2/\text{c}$ phase transition in alkaline-earth feldspars along the $\text{CaAl}_2\text{Si}_2\text{O}_8\text{-SrAl}_2\text{Si}_2\text{O}_8$ join: Thermodynamic behaviour. *Physics and Chemistry of Minerals*, 20, 221–227.
- (2000) TEM observations on the $\text{P}\bar{1}$ - $\text{I}\bar{1}$ phase transition in feldspars along the join $\text{CaAl}_2\text{Si}_2\text{O}_8\text{-SrAl}_2\text{Si}_2\text{O}_8$. *American Mineralogist*, 85, 963–970.
- Winter, J.K., Okamura, F.P., and Ghose, S. (1979) A high-temperature structural study of high albite, monalbite, and the analbite-monalbite phase transition. *American Mineralogist*, 64, 409–423.

MANUSCRIPT RECEIVED DECEMBER 9, 2002

MANUSCRIPT ACCEPTED MAY 12, 2003

MANUSCRIPT HANDLED BY ALESSANDRO GUALTIERI